

# Stability Analysis of Simple Running Models

Ken

June, 2018\*

## 1 Introduction

The purpose of this project is to analyze the stability (via Poincare map) of three simple running models to get a better understanding to the source of stability and robustness for fast runners. The three simple runners are:

- 2 DOF (Vertical) Hopper with pitch angle control
- Spring Loaded Inverted Pendulum (SLIP) model
- SLIP with Pendulum Runner (SLIPPER)

### 1.1 About the systems

In this analysis, all the models are 2D runners. The following are important common assumptions applied to all simple running models in this project

- Massless leg – No impact will be induced during foot collision.
- Energy conservation (especially for passive runners)
- Open-loop control on leg (e.g. open-loop leg force, or fixed touch-down angle for SLIP-based runners)
- Closed-loop control on pitch angle

Important parameters or quantities

- Spring stiffness
- Running speed/running period/running frequency
- Duty factor =  $\frac{t_{stance}}{t_{stance} + t_{flight}}$
- Fast running index (proposed by IHMC)

Other important concepts (of fast runner)

- Meta center
- Resonance – Please check Jorge Cham's thesis [11] 2.2 Resonance in Running.
- Please refer to fast runner meeting notes or proposal for more information.

---

\*Last update: August 23, 2018

## **1.2 Related research**

- Jorge Cham's Dissertation
- David Remy's Dissertation
- Shan's paper

## **1.3 About the method of stability analysis used in this project**

**Some "must-have" and "nice-to-have" requirements for the analysis method**

- Stability analysis
- Robustness
- Dimension analysis (so that it can be used for robots with different scales)
- Applicable to complex system (e.g. for the designed mechanism)

For the requirements listed above, and also to explore the nonlinearity and coupled dynamics for SLIP-based runners, the main method for stability analysis used in this project contains two parts:

- Trajectory optimization using single-shooting method – For finding periodic motions.
- Poincare Map – Check the Eigen values of the Poincare map (it is a matrix) of a periodic motion to determine its stability (i.e. a stable limit cycle or unstable one).

### **1.3.1 About the Poincare section and Poincare map**

### **1.3.2 About the Trajectory optimization using single shooting method**

## **1.4 Fast running index**

## **1.5 ToDo**

## 2 Pitch Stability of an Vertically Open-loop Hopper

### 2.1 Jorge Cham's Dissertation - openloop control of 1DOF vertical hopper

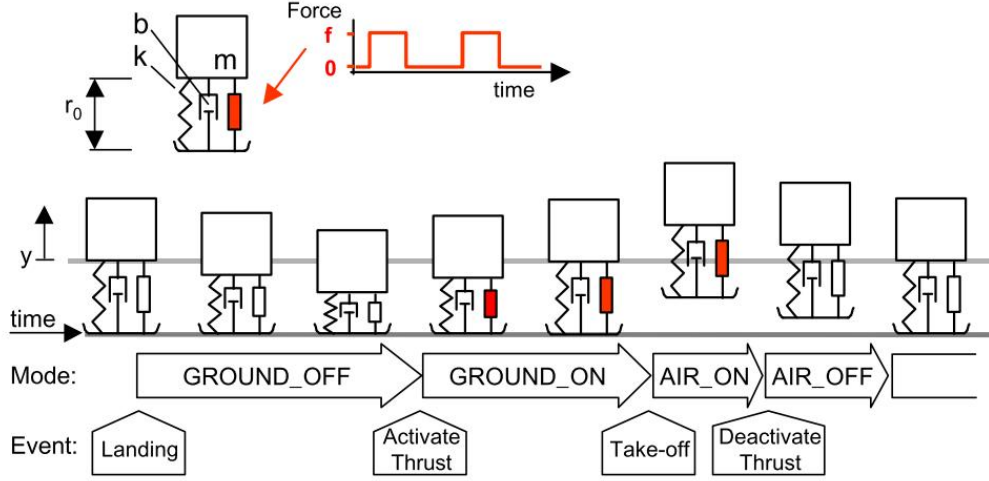


**Figure 3-1.** The vertical hopping model used for analysis. The hopper's leg consists of a spring, a damper and a force element which is active according to a binary motor pattern. The figure shows a sample trajectory of the hopper, the different modes that it goes through, and the events that trigger the transitions between the modes.

Figure 1: The schematic of a 1 DOF hopper [11]

#### 2.1.1 Equation of motion

Using the model as shown in Fig. 1, during the stand phase (i.e.  $y \leq 0$ ), the equation of motion can be expressed as:

$$m\ddot{y} = -b\dot{y} - ky - mg + f$$

where  $m$  is the mass,  $b$  is the damping,  $k$  is the stiffness,  $f$  is the control input. Normalized by weight, the equation becomes

$$\ddot{y} = -b/m\dot{y} - k/my - g + f/m$$

Expressed in state space form:

$$\begin{bmatrix} \dot{y} \\ \ddot{y} \end{bmatrix} = \begin{bmatrix} 0 & 1 \\ -k/m & -b/m \end{bmatrix} \begin{bmatrix} y \\ \dot{y} \end{bmatrix} + \begin{bmatrix} 0 \\ -g + f/m \end{bmatrix} \quad (1)$$

or equivalently

$$\dot{X} = \begin{bmatrix} 0 & 1 \\ -\omega^2 & -2\xi\omega \end{bmatrix} X + \begin{bmatrix} 0 \\ -g + f_n(t) \end{bmatrix} = \begin{bmatrix} 0 & 1 \\ -k_p & -k_d \end{bmatrix} X + \begin{bmatrix} 0 \\ -g + f_n(t) \end{bmatrix} \quad (2)$$

where  $X \triangleq [y, \dot{y}]^T$ . When the hopper is in the air (i.e.  $y > 0$ , flight phase),

$$\dot{X} = \begin{bmatrix} 0 & 1 \\ 0 & 0 \end{bmatrix} X + \begin{bmatrix} 0 \\ -g \end{bmatrix} \quad (3)$$

Define the force of an open-loop motor pattern

$$f_n(t) = \begin{cases} f/m, & \text{if } t_{off} < t < t_{off} + t_{on}. \\ 0, & \text{otherwise.} \end{cases} \quad (4)$$

## 2.2 Stability Analysis of an Open-loop Controlled Hopper with Discrete Pitch Angle Control

Use the state space of z motion form 2 with a simplified open-loop force input:

$$\begin{bmatrix} \dot{z} \\ \ddot{z} \end{bmatrix} = \begin{bmatrix} 0 & 1 \\ -kp_z & -kd_z \end{bmatrix} \begin{bmatrix} z \\ \dot{z} \end{bmatrix} + \begin{bmatrix} 0 \\ -g + f_n(t) \end{bmatrix} \quad (5)$$

where

$$f_n(t) = \begin{cases} f_n \triangleq f/m, & \text{if } t_{flight} < t < t_{flight} + t_{contact}. \\ 0, & \text{otherwise.} \end{cases} \quad (6)$$

To further simplify the problem, assuming  $f_n(t)$  is much more dominant than  $-kp_z z - kd_z \dot{z} - g$  so that:

$$\begin{bmatrix} \dot{z} \\ \ddot{z} \end{bmatrix} \approx \begin{bmatrix} 0 & 1 \\ 0 & 0 \end{bmatrix} \begin{bmatrix} z \\ \dot{z} \end{bmatrix} + \begin{bmatrix} 0 \\ f_n(t) \end{bmatrix} \quad (7)$$

Assumptions:

- $f_n(t)$ <sup>1</sup> can induce stable vertical hopping motion.
- $t_0$  starts when the foot leaves the ground.
- $t_{flight} + t_{contact} = T$ ,  $t_{contact} = \alpha$ , and  $T > \alpha$

Then the pitch dynamics with feedback control can be expressed as:

$$\begin{bmatrix} \dot{\theta} \\ \ddot{\theta} \end{bmatrix} = \begin{bmatrix} 0 & 1 \\ 0 & 0 \end{bmatrix} \begin{bmatrix} \theta \\ \dot{\theta} \end{bmatrix} + \begin{bmatrix} 0 \\ -f_n(t)m/I\Delta x \end{bmatrix} \quad (8)$$

### 2.2.1 Poincare Section

Denote the state at the  $n^{th}$  step Poincare section  $\theta_n, \dot{\theta}_n$  (defined at the start of the flight phase). Then we can calculate the state at Poincare section at the  $n+1^{th}$  step:

$$\dot{\theta}_{n+1} = \dot{\theta}_n - \frac{f}{I} \Delta x t_{contact} \quad (9)$$

$$\theta_{n_{touchDown}} = \theta_n + \dot{\theta}_n t_{flight}$$

$$\dot{\theta}_{n_{touchDown}} = \dot{\theta}_n$$

$$\begin{aligned} \theta_{n+1} &= \theta_n + \dot{\theta}_n t_{flight} + \dot{\theta}_n t_{contact} - \frac{1}{2} \frac{f}{I} \Delta x t_{contact}^2 \\ &= \theta_n + T \dot{\theta}_n - \frac{1}{2} \frac{f}{I} \alpha^2 \Delta x \end{aligned} \quad (10)$$

### 2.2.2 Poincare Map of Pitch Dynamics with Proportional Control

By designing a proportional control such that  $\Delta x = k\phi_n$  and defining  $K = \frac{1}{2} \frac{f}{I} k$ , Eq. 9 and Eq.10 can be expressed as follows:

$$\begin{aligned} \theta_{n+1} &= \theta_n - \alpha^2 K \theta_n + T \dot{\theta}_n \\ \dot{\theta}_{n+1} &= \dot{\theta}_n - 2\alpha K \theta_n \end{aligned}$$

---

<sup>1</sup>Conceptually, the  $f_n(t)$  can be treated as a force applied from a nonlinear component which connects the massless leg to the body (so there is no velocity change happen at foot strike)

Arranged them in the state space equation, we can get a discrete map  $M$  (i.e. Poincare Map, with set of difference equations):

$$\begin{bmatrix} \theta_{n+1} \\ \dot{\theta}_{n+1} \end{bmatrix} = \begin{bmatrix} 1 - \alpha^2 K & T \\ -2\alpha K & 1 \end{bmatrix} \begin{bmatrix} \theta_n \\ \dot{\theta}_n \end{bmatrix} = M \begin{bmatrix} \theta_n \\ \dot{\theta}_n \end{bmatrix} \quad (11)$$

### Eigen value analysis

To analyze the stability of the equation in 11, we need to check whether the eigen values of Poincare map  $M$  are within the unit cycle. Similar to the Routh-Herwitz method for the continuous map, we can use Jury Stability Test (Ogata, 1985)<sup>2</sup>, which states that a discrete system of two dimensions with the characteristic equations  $P(z)$  of the form:

$$P(z) = a_0 z^2 + a_1 z + a_2$$

where  $a_0 > 0$ , is stable if the following conditions are all satisfied:

$$\begin{aligned} |a_2| &< a_0 \\ a_0 + a_1 + a_2 &> 0 \\ a_0 - a_1 + a_2 &> 0 \\ |(a_0 + a_2)(a_2 - a_0)| &> |a_1(a_0 - a_1)| \end{aligned}$$

For a Jacobian of the form

$$J = \begin{bmatrix} J_1 & J_2 \\ J_3 & J_4 \end{bmatrix}$$

The characteristics equation can be expressed as follows:

$$P(z) = z^2 - (J_1 + J_4)z + (J_1 J_4 - J_2 J_3)$$

Substituting into the stable conditions stated above,

$$|(J_1 J_4 - J_2 J_3)| < 1 \quad (12)$$

$$1 - (J_1 + J_4) + (J_1 J_4 - J_2 J_3) > 0 \quad (13)$$

$$1 + (J_1 + J_4) + (J_1 J_4 - J_2 J_3) > 0 \quad (14)$$

$$|(1 + (J_1 J_4 - J_2 J_3))((J_1 J_4 - J_2 J_3) - 1)| > |(J_1 + J_4)(1 + (J_1 + J_4))| \quad (15)$$

### Check condition Eq.12:

First assuming  $1 - \alpha^2 K + 2T\alpha K > 0$

$$\begin{aligned} 1 - \alpha^2 K + 2T\alpha K &< 1 \\ \rightarrow -\alpha^2 K + 2T\alpha K &< 0 \\ \rightarrow \alpha K(-\alpha + 2T) &< 0 \end{aligned}$$

Since  $\alpha > 0$ ,  $K > 0$ , and  $T > \alpha$ , the assumption cannot satisfy the condition.

Next, assuming  $1 - \alpha^2 K + 2T\alpha K < 0$  :

$$\begin{aligned} 1 - \alpha^2 K + 2T\alpha K &> -1 \\ \rightarrow -1 + \alpha^2 K - 2T\alpha K &< 1 \\ \rightarrow \alpha K(\alpha - 2T) &< 2 \end{aligned}$$

---

<sup>2</sup>contents quoted from [11]

Since  $T > \alpha$ , the condition can always be satisfied, as long as the following condition is satisfied:

$$(J_1 J_4 - J_2 J_3) = (1 - \alpha^2 K + 2T\alpha K) < 0$$

Combine conditions above we can get a new inequality as follows:

$$-1 < (J_1 J_4 - J_2 J_3) = (1 - \alpha^2 K + 2T\alpha K) < 0 \quad (16)$$

**Check condition Eq.13:**

$$\begin{aligned} 1 - (1 - \alpha^2 K + 1) + (1 - \alpha^2 K + 2T\alpha K) &> 0 \\ &\rightarrow 2T\alpha K > 0 \end{aligned}$$

From the last inequality we can get the condition is always hold.

**Check condition Eq.14:**

$$\begin{aligned} 1 + (1 - \alpha^2 K + 1) + (1 - \alpha^2 K + 2T\alpha K) &> 0 \\ &\rightarrow 4 - 2\alpha^2 K + 2T\alpha K > 0 \\ &\rightarrow 4 + \alpha K(-2\alpha + 2T) > 0 \end{aligned}$$

From the last inequality we can get the condition is always hold.

**Check condition Eq.15:**

Based on Eq. 16, the left hand side of Eq. 15 can be rearranged as :

$$|(det(M) + 1)(det(M) - 1)| = |det(M)^2 - 1| = 1 - det(M)^2$$

From Eq. 13 and 14 we can got  $(J_1 + J_4) > 0$ , therefore the right hand side of Eq. 15 can be rearranged as:

$$|(J_1 + J_4)(J_1 + J_4 + 1)| = (J_1 + J_4)(J_1 + J_4 + 1)$$

Therefore the Eq. 15 can be expressed as follows:

$$1 - det(M)^2 > tr(M)(tr(M) + 1)$$

where  $det(M) = \prod_i \lambda_i = (J_1 J_4 - J_2 J_3)$  is the determinant of matrix  $M$  and  $tr(M) = \sum_i \lambda_i = (J_1 + J_4)$  is the trace of the matrix  $M$ .

**To sum up**

For the (Poincare) stability, the following conditions need to be satisfied:

$$-1 < det(M) < 0 \quad (17)$$

$$0 < tr(M)(tr(M) + 1) < 1 - det(M)^2 \quad (18)$$

where

$$\begin{aligned} det(M) &= 1 - \alpha^2 K + 2T\alpha K \\ tr(M) &= 2 - \alpha^2 K \\ K &= \frac{1}{2} \frac{f_n}{I} k \end{aligned}$$

**Result**

After check the sign of the  $det(M)$ , it was found that  $det(M)$  always  $> 0$ :

$$1 - \alpha^2 K + 2T\alpha K = 1 + \alpha K(-\alpha + 2T) > 0$$

Therefore, it is concluded that proportional control with this system setup cannot stabilize the pitch dynamics.

### 2.2.3 Poincare Map of Pitch Dynamics with PD Control

By designing a PD control such that  $\Delta x = k_p \theta_n + k_d \dot{\theta}_n$  and defining  $K = \frac{1}{2} \frac{f}{I} k_p$ ,  $C = \frac{1}{2} \frac{f}{I} k_d$ , Eq. 9 and Eq.10 can be expressed as follows:

$$\begin{aligned}\theta_{n+1} &= \theta_n - \alpha^2 K \theta_n + T \dot{\theta}_n - \alpha^2 C \dot{\theta}_n \\ \dot{\theta}_{n+1} &= \dot{\theta}_n - 2\alpha K \theta_n - 2\alpha C \dot{\theta}_n\end{aligned}$$

Arranged them in the state space equation, we can get a discrete map  $M_{pd}$ :

$$\begin{bmatrix} \theta_{n+1} \\ \dot{\theta}_{n+1} \end{bmatrix} = \begin{bmatrix} 1 - \alpha^2 K & T - \alpha^2 C \\ -2\alpha K & 1 - 2\alpha C \end{bmatrix} \begin{bmatrix} \theta_n \\ \dot{\theta}_n \end{bmatrix} = M_{pd} \begin{bmatrix} \theta_n \\ \dot{\theta}_n \end{bmatrix} \quad (19)$$

### 2.2.4 Analytical Solution for Eq.7

Start from  $t_0$  (the beginning of the flight phase), assuming  $Z = [0, \dot{z}_0]^T$ , then we can get:

$$z(t_{flight}) = \dot{z}_0 t_{flight} - 1/2 g t_{flight}^2 = 0 \quad (20)$$

$$\dot{z}(t_{flight}) = \dot{z}_0 - g t_{flight} = -\dot{z}_0 \quad (21)$$

where a constraint for the  $\dot{z}_0$  can be derived:

$$\dot{z}_0 = 1/2 g t_{flight} \quad (22)$$

$$(23)$$

Then we can derive the solution at the end of the touch down:

$$z(1) = -\dot{z}_0 t_{contact} + (f/m - g) t_{contact}^2 = 0 \quad (24)$$

$$\dot{z}(1) = -\dot{z}_0 + (f/m - g) t_{contact} = \dot{z}_0 \quad (25)$$

where another constraint for the  $\dot{z}_0$  can be derived:

$$\dot{z}_0 = 1/2 (f/m - g) t_{contact} \quad (26)$$

**Period  $T$ , contact force  $f$  and  $t_{contact}$  are dependent** From Eqs. 26 and 22 we can get

$$\begin{aligned} 1/2 g t_{flight} &= 1/2 (f/m - g) t_{contact} \\ \rightarrow t_{flight} &= (f/mg - 1) t_{contact} \\ \rightarrow t_{flight} + t_{contact} &= T = (f/mg) t_{contact} \end{aligned}$$



## 2.3 Stability Analysis of an Open-loop Controlled Hopper with Continuous Pitch Angle Control

Consider the case that  $\Delta x = k\theta(t)$  or  $\Delta x = k_p\theta(t) + k_d\dot{\theta}(t)$ , then the pitch angle will be controlled continuously in the stance phase.

### 2.3.1 Poincare map of Hopper with Continuous Proportional Control

Assuming  $\Delta x = k\theta(t)$ , then the system dynamic in the stance phase becomes:

$$\dot{X} = \begin{bmatrix} \dot{\theta} \\ \ddot{\theta} \end{bmatrix} = \begin{bmatrix} 0 & 1 \\ -k\frac{f}{I} & 0 \end{bmatrix} X \triangleq \begin{bmatrix} 0 & 1 \\ -2K & 0 \end{bmatrix} X = AX \quad (27)$$

where  $K = \frac{1}{2}\frac{f}{I}k$ . Again denoting the state at the  $n^{th}$  step Poincare section  $X_n = [\theta_n, \dot{\theta}_n]^T$  (defined at the start of the flight phase). Then we can first calculate the touchdown state at  $n_{th}$  step:

$$\begin{aligned} \theta_{nTD} &= \theta_n + \dot{\theta}_n t_{flight} \\ \dot{\theta}_{nTD} &= \dot{\theta}_n \end{aligned}$$

and  $X_{nTD} = [\theta_{nTD}, \dot{\theta}_{nTD}]^T$  then can be expressed as:

$$X_{nTD} = \begin{bmatrix} 1 & (T - \alpha) \\ 0 & 1 \end{bmatrix} X_n \quad (28)$$

Next, assuming the contact time is exactly  $t_{contact} = \alpha$  (e.g. no perturbation in  $z$  direction), then the  $X_{n+1} = [\theta_{n+1}, \dot{\theta}_{n+1}]^T$  can be expressed with  $X_{nTD} = [\theta_{nTD}, \dot{\theta}_{nTD}]^T$ :

$$X_{n+1} = e^{A\alpha}(X_{nTD} - X_{eq}) + X_{eq} \quad (29)$$

$$= e^{A\alpha} \left( \begin{bmatrix} 1 & (T - \alpha) \\ 0 & 1 \end{bmatrix} X_n - X_{eq} \right) + X_{eq} \quad (30)$$

where  $X_{eq} = [0, 0]^T$  is the equilibrium point of Eq. 27. Therefore, we can get the Poincare map in this case is:

$$M = e^{A\alpha} \left( \begin{bmatrix} 1 & (T - \alpha) \\ 0 & 1 \end{bmatrix} \right) \quad (31)$$

Using symbolic tool in MATLAB, we can derive the closed-form expression of  $M$  as follows:

$$M = \begin{bmatrix} M_{11} & M_{12} \\ M_{21} & M_{22} \end{bmatrix}$$

where

$$\begin{aligned} M_{11} &= \frac{e^{\sqrt{2}\sqrt{-K}a}}{2} + \frac{e^{-\sqrt{2}\sqrt{-K}a}}{2} \\ M_{12} &= \left( \frac{e^{\sqrt{2}\sqrt{-K}a}}{2} + \frac{e^{-\sqrt{2}\sqrt{-K}a}}{2} \right) (T - a) + \frac{\sqrt{2}e^{\sqrt{2}\sqrt{-K}a} - \sqrt{2}e^{-\sqrt{2}\sqrt{-K}a}}{4\sqrt{-K}} \\ M_{21} &= \frac{\sqrt{2}\sqrt{-K}e^{\sqrt{2}\sqrt{-K}a}}{2} - \frac{\sqrt{2}\sqrt{-K}e^{-\sqrt{2}\sqrt{-K}a}}{2} \\ M_{22} &= \frac{e^{\sqrt{2}\sqrt{-K}a}}{2} + \frac{e^{-\sqrt{2}\sqrt{-K}a}}{2} + \left( \frac{\sqrt{2}\sqrt{-K}e^{\sqrt{2}\sqrt{-K}a}}{2} - \frac{\sqrt{2}\sqrt{-K}e^{-\sqrt{2}\sqrt{-K}a}}{2} \right) (T - a) \end{aligned}$$

### 2.3.2 Poincare Map of Hopper with Continuous PD Control

Assuming  $\Delta x = k_p \theta(t) + k_d \dot{\theta}(t)$ , then the system dynamic in the stance phase becomes:

$$\dot{X} = \begin{bmatrix} \dot{\theta} \\ \ddot{\theta} \end{bmatrix} = \begin{bmatrix} 0 & 1 \\ -k_p \frac{f}{I} & -k_d \frac{f}{I} \end{bmatrix} X \triangleq \begin{bmatrix} 0 & 1 \\ -2K & -2C \end{bmatrix} X = AX \quad (32)$$

$$M_{pd} = e^{A\alpha} \begin{bmatrix} 1 & (T - \alpha) \\ 0 & 1 \end{bmatrix} \quad (33)$$

Using symbolic tool in MATLAB, we can derive the closed-form expression of  $M_{pd}$  as follows:

$$M_{pd} = \begin{bmatrix} M_{11} & M_{12} \\ M_{21} & M_{22} \end{bmatrix}$$

where

$$\begin{aligned} M_{11} &= \frac{C e^{a\sqrt{C^2-2K}-Ca} - C e^{-Ca-a\sqrt{C^2-2K}} + e^{a\sqrt{C^2-2K}-Ca} \sqrt{C^2-2K} + e^{-Ca-a\sqrt{C^2-2K}} \sqrt{C^2-2K}}{2\sqrt{C^2-2K}} \\ M_{12} &= \frac{e^{a\sqrt{C^2-2K}-Ca} - e^{-Ca-a\sqrt{C^2-2K}}}{2\sqrt{C^2-2K}} + \\ &\quad \frac{(T-a) \left( C e^{a\sqrt{C^2-2K}-Ca} - C e^{-Ca-a\sqrt{C^2-2K}} + e^{a\sqrt{C^2-2K}-Ca} \sqrt{C^2-2K} + e^{-Ca-a\sqrt{C^2-2K}} \sqrt{C^2-2K} \right)}{2\sqrt{C^2-2K}} \\ M_{21} &= - \frac{K e^{a\sqrt{C^2-2K}-Ca} - K e^{-Ca-a\sqrt{C^2-2K}}}{\sqrt{C^2-2K}} \\ M_{22} &= \frac{C e^{-Ca-a\sqrt{C^2-2K}} - C e^{a\sqrt{C^2-2K}-Ca} + e^{a\sqrt{C^2-2K}-Ca} \sqrt{C^2-2K} + e^{-Ca-a\sqrt{C^2-2K}} \sqrt{C^2-2K}}{2\sqrt{C^2-2K}} - \\ &\quad \frac{(T-a) \left( K e^{a\sqrt{C^2-2K}-Ca} - K e^{-Ca-a\sqrt{C^2-2K}} \right)}{\sqrt{C^2-2K}} \end{aligned}$$

### 2.3.3 General Solution of Poincare Map of Hybrid Linear Systems

$$\dot{Z} = AZ + B \quad (34)$$

where **A is invertible**. If the **mode transistion is time-based**, then we can augment the state of the system with  $t$ :

$$\dot{X} = \begin{bmatrix} \dot{t} \\ \dot{Z} \end{bmatrix} = \begin{bmatrix} 0 & 0 \\ 0 & A \end{bmatrix} X + \begin{bmatrix} 1 \\ B \end{bmatrix} \quad (35)$$

where  $X = [t, Z]^T$ . Assuming the mode trasition happened under the following condition:

$$e^T X = 0 \quad (36)$$

and takes time  $\Delta t$  from  $X_n$  to  $X_{n+1}$ , then the Poincare map (Jacobian matrix) can be expressed as:

$$\frac{\partial X_{n+1}}{\partial X_n} = -\dot{X}_{n+1}(e^T \dot{X}_{n+1})^{-1}e^T \begin{bmatrix} 1 & 0 \\ 0 & e^{A\Delta t} \end{bmatrix} + \begin{bmatrix} 1 & 0 \\ 0 & e^{A\Delta t} \end{bmatrix} \quad (37)$$

### 3 2D Spoked Runners

Extended from the vertical hopper, this model is aimed to use for analysis of coupled dynamics of the spoked runner, which has following assumptions

- massless leg

#### 3.1 SLIP model with a locked flywheel

Compared to [XXX], this is a model which is generalized so that the rotation in the flight phase can also be considered.

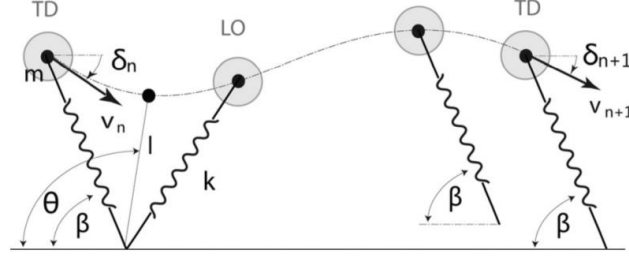


**Fig. 1** The SLIP model. The parameters  $m$ ,  $k$ , and  $\beta$  stand for body mass, leg stiffness, and landing angle, respectively. The CoM position during stance is characterized by leg length  $l$  and leg angle  $\theta$ . Here, TD and LO stand for touchdown and liftoff, respectively.

Figure 2: The schematic of a SLIP model

##### 3.1.1 System Kinematics

As indicated in Fig 2, the position of the body (mass) is

$$\begin{aligned} x &= -l \cos \theta \\ z &= l \sin \theta \end{aligned}$$

and the velocity

$$\begin{aligned} \dot{x} &= -\dot{l} \cos \theta + l \sin \theta \dot{\theta} \\ \dot{z} &= \dot{l} \sin \theta + l \cos \theta \dot{\theta} \end{aligned}$$

##### 3.1.2 Lagrangian Mechanics

With the velocity of the mass, the Lagrangian  $L$  can be expressed as:

$$\begin{aligned} L &= T - V = \frac{1}{2} m (\dot{x}^2 + \dot{z}^2) + \frac{1}{2} I \dot{\theta}^2 - V_{spring} - V_{gravity} \\ &= \frac{1}{2} m (\dot{l}^2 + l^2 \dot{\theta}^2) + \frac{1}{2} I \dot{\theta}^2 - \frac{1}{2} k (l - l_0)^2 - mg(l \sin \theta) \end{aligned}$$

where  $I = mr_g^2$ . Take  $l$ ,  $\theta$  as the generalized coordinate, the equation of motions are:

**Stance Dynamics**

$$\begin{aligned} m \ddot{l} - m l^2 \ddot{\theta} + k(l - l_0) &= -mg \sin \theta \\ 2m l \dot{l} \dot{\theta} + m(l^2 + r_g^2) \ddot{\theta} &= -m g l \cos \theta \end{aligned}$$

## Flight Dynamics

$$\begin{aligned}
 \ddot{y} &= -g \\
 \ddot{\theta} &= 0 \\
 \text{LO: } l &= l_0 \\
 \text{TD: } y &= l_0 \sin \beta \\
 (\text{Spoked TD: } \theta &= \beta + \frac{2\pi}{d})
 \end{aligned}$$

where  $\beta$  is the touch down angle,  $d$  is the number of the legs the spoked runner has.

**Note:** when  $I = 0$ , the system is equivalent to the transitional SLIP model as described in [XXX].

### 3.1.3 EOM of SLIP model with a locked fly wheel

This is an extended model which is used for the stability analysis of the 2D spoked (or reciprocating) runner.

**Note:** In the flight phase there will be the inertia at COM (the two masses connected via the link with length  $r_c$ ), therefore no flywheel is required for the rotation EOM.

## 3.2 SLIP model with a pendulum

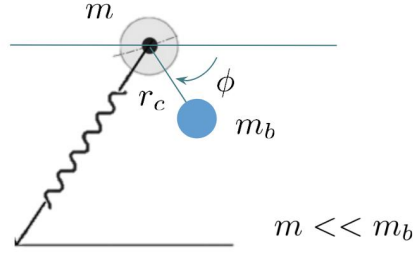


Figure 3: The schematic of a SLIP model

### 3.2.1 System Kinematics

As indicated in Fig 3, the position and the velocity of the frame  $m$  are:

$$\begin{aligned}
 x &= -l \cos \theta \\
 z &= l \sin \theta \\
 \dot{x} &= -\dot{l} \cos \theta + l \sin \theta \dot{\theta} \\
 \dot{z} &= \dot{l} \sin \theta + l \cos \theta \dot{\theta}
 \end{aligned}$$

The position and the velocity of the body  $m_b$  are:

$$\begin{aligned}
 x_b &= -l \cos \theta + r_c \cos(\phi) \\
 z_b &= l \sin \theta - r_c \sin(\phi) \\
 \dot{x}_b &= -\dot{l} \cos \theta + l \sin \theta \dot{\theta} - r_c \sin(\phi) (\dot{\phi}) \\
 \dot{z}_b &= \dot{l} \sin \theta + l \cos \theta \dot{\theta} - r_c \cos(\phi) (\dot{\phi})
 \end{aligned}$$

### 3.2.2 Lagrangian Mechanics

With the velocity of the masses, the Lagrangian  $L$  can be expressed as:

$$\begin{aligned} L = T - V &= \frac{1}{2}m(\dot{x}^2 + \dot{z}^2) + \frac{1}{2}m_b(\dot{x}_b^2 + \dot{z}_b^2) - V_{spring} - V_{gravity} - V_{b_{gravity}} \\ &= \frac{1}{2}m(\dot{l}^2 + l^2\dot{\theta}^2) + \frac{1}{2}m_b(\dot{l}^2 + l^2\dot{\theta}^2 + r_c^2\dot{\phi}^2 + 2\dot{\phi}r_c(l\sin(\phi - \theta) - l\dot{\theta}\cos(\phi - \theta))) \\ &\quad - \frac{1}{2}k(l - l_0)^2 - mg(l\sin\theta) - m_bg(l\sin\theta - r_c\sin\phi) \end{aligned}$$

EOM of  $l$ :

$$\begin{aligned} \frac{\partial L}{\partial l} &= -(m + m_b)g\sin\theta + (m + m_b)l\dot{\theta}^2 - k(l - l_0) - m_br_c\dot{\phi}\dot{\theta}\cos(\phi - \theta) \\ \frac{\partial L}{\partial \dot{l}} &= (m + m_b)\dot{l} + m_br_c\dot{\phi}\sin(\phi - \theta) \\ \frac{d}{dt}\frac{\partial L}{\partial \dot{l}} &= (m + m_b)\ddot{l} + m_br_c\ddot{\phi}\sin(\phi - \theta) + m_br_c\dot{\phi}\cos(\phi - \theta)(\dot{\phi} - \dot{\theta}) \end{aligned}$$

EOM of  $\theta$ :

$$\begin{aligned} \frac{\partial L}{\partial \theta} &= -(m + m_b)gl\cos\theta + m_br_c\dot{\phi}(-\dot{l}\cos(\phi - \theta) - l\dot{\theta}\sin(\phi - \theta)) \\ \frac{\partial L}{\partial \dot{\theta}} &= (m + m_b)l^2\dot{\theta} - m_br_c\dot{\phi}l\cos(\phi - \theta) \\ \frac{d}{dt}\frac{\partial L}{\partial \dot{\theta}} &= (m + m_b)l^2\ddot{\theta} + 2(m + m_b)l\dot{l}\dot{\theta} \\ &\quad - m_br_c\ddot{\phi}\cos(\phi - \theta) - m_br_c\dot{\phi}\dot{l}\cos(\phi - \theta) + m_br_c\dot{\phi}l\sin(\phi - \theta)(\dot{\phi} - \dot{\theta}) \end{aligned}$$

EOM of  $\phi$ :

$$\begin{aligned} \frac{\partial L}{\partial \phi} &= m_bg r_c \cos(\phi) + m_br_c\dot{\phi}(l\cos(\phi - \theta) + l\dot{\theta}\sin(\phi - \theta)) \\ \frac{\partial L}{\partial \dot{\phi}} &= m_br_c^2(\dot{\phi}) + m_br_c(l\sin(\phi - \theta) - l\dot{\theta}\cos(\phi - \theta)) \\ \frac{d}{dt}\frac{\partial L}{\partial \dot{\phi}} &= m_br_c^2(\ddot{\phi}) + m_br_c(\ddot{l}\sin(\phi - \theta) + \dot{l}\cos(\phi - \theta)(\dot{\phi} - \dot{\theta})) \\ &\quad - m_br_c(\dot{l}\dot{\theta}\cos(\phi - \theta) + l\ddot{\theta}\cos(\phi - \theta) - l\dot{\theta}\sin(\phi - \theta)(\dot{\phi} - \dot{\theta})) \end{aligned}$$

Take  $l$ ,  $\theta$ ,  $\phi$  as the generalized coordinate, the equation of motions are:

$$\begin{aligned} (m + m_b)\ddot{l} + m_br_c\ddot{\phi}\sin(\phi - \theta) + m_br_c\dot{\phi}\cos(\phi - \theta)(\dot{\phi} - \dot{\theta}) &= \\ - (m + m_b)g\sin\theta + (m + m_b)l\dot{\theta}^2 - k(l - l_0) - m_br_c\dot{\phi}\dot{\theta}\cos(\phi - \theta) & \\ (m + m_b)l^2\ddot{\theta} + 2(m + m_b)l\dot{l}\dot{\theta} - m_br_c\ddot{\phi}\cos(\phi - \theta) - m_br_c\dot{\phi}\dot{l}\cos(\phi - \theta) + m_br_c\dot{\phi}l\sin(\phi - \theta)(\dot{\phi} - \dot{\theta}) &= \\ - (m + m_b)gl\cos\theta + m_br_c\dot{\phi}(-\dot{l}\cos(\phi - \theta) - l\dot{\theta}\sin(\phi - \theta)) & \\ m_br_c^2(\ddot{\phi}) + m_br_c(\ddot{l}\sin(\phi - \theta) + \dot{l}\cos(\phi - \theta)(\dot{\phi} - \dot{\theta})) - m_br_c(\dot{l}\dot{\theta}\cos(\phi - \theta) + l\ddot{\theta}\cos(\phi - \theta) - l\dot{\theta}\sin(\phi - \theta)(\dot{\phi} - \dot{\theta})) &= \\ m_bg r_c \cos(\phi) + m_br_c\dot{\phi}(l\cos(\phi - \theta) + l\dot{\theta}\sin(\phi - \theta)) & \end{aligned}$$

Rearrange the EOMs and move all terms without accelerations to the right hand side:

$$\begin{aligned}
& \ddot{l}(m + m_b) + \ddot{\phi}m_b r_c \sin(\phi - \theta) = \\
& - m_b r_c \dot{\phi} \cos(\phi - \theta)(\dot{\phi} - \dot{\theta}) - (m + m_b)g \sin \theta + (m + m_b)l\dot{\theta}^2 - k(l - l_0) - m_b r_c \dot{\phi} \dot{\theta} \cos(\phi - \theta) \\
& \ddot{\theta}(m + m_b)l^2 - \ddot{\phi}m_b r_c \cos(\phi - \theta) = \\
& - 2(m + m_b)l\dot{\theta} + m_b r_c \dot{\phi} \dot{\theta} \cos(\phi - \theta) - m_b r_c \dot{\phi} \sin(\phi - \theta)(\dot{\phi} - \dot{\theta}) - (m + m_b)g \cos \theta + m_b r_c \dot{\phi}(-\dot{\theta} \cos(\phi - \theta) - l\dot{\theta} \sin(\phi - \theta)) \\
& \ddot{\phi}m_b r_c^2 + \ddot{l}m_b r_c \sin(\phi - \theta) - \ddot{\theta}m_b r_c l \cos(\phi - \theta) = \\
& - m_b r_c \dot{\theta} \cos(\phi - \theta)(\dot{\phi} - \dot{\theta}) + m_b r_c(l\dot{\theta} \cos(\phi - \theta) - l\dot{\theta} \sin(\phi - \theta)(\dot{\phi} - \dot{\theta})) \\
& + m_b g r_c \cos(\phi) + m_b r_c \dot{\phi}(l \cos(\phi - \theta) + l\dot{\theta} \sin(\phi - \theta))
\end{aligned}$$

Equation of motion of the stance phase in matrix form:

$$\begin{aligned}
\ddot{X} &= \begin{bmatrix} \ddot{l} \\ \ddot{\theta} \\ \ddot{\phi} \end{bmatrix} \\
&= M^{-1} \begin{bmatrix} -mr_c \dot{\phi} \cos(\phi - \theta)(\dot{\phi} - \dot{\theta}) - (m_f + m)g \sin \theta + (m_f + m)l\dot{\theta}^2 - k(l - l_0) - mr_c \dot{\phi} \dot{\theta} \cos(\phi - \theta) \\ -2(m_f + m)l\dot{\theta} + mr_c \dot{\phi} \dot{\theta} \cos(\phi - \theta) - mr_c \dot{\phi} \sin(\phi - \theta)(\dot{\phi} - \dot{\theta}) - (m_f + m)g \cos \theta + mr_c \dot{\phi}(-\dot{\theta} \cos(\phi - \theta) - l\dot{\theta} \sin(\phi - \theta)) \\ -mr_c \dot{\theta} \cos(\phi - \theta)(\dot{\phi} - \dot{\theta}) + mr_c(l\dot{\theta} \cos(\phi - \theta) - l\dot{\theta} \sin(\phi - \theta)(\dot{\phi} - \dot{\theta})) + m g r_c \cos(\phi) + mr_c \dot{\phi}(l \cos(\phi - \theta) + l\dot{\theta} \sin(\phi - \theta)) \end{bmatrix} \quad (1)
\end{aligned}$$

LO:  $l = l_0$  (2)

where  $M$  is the inertia matrix:

$$M = \begin{bmatrix} m + m_f & 0 & mr_c \sin(\phi - \theta) \\ 0 & (m + m_f)l^2 & -mr_c \cos(\phi - \theta) \\ mr_c \sin(\phi - \theta) & -mr_c \cos(\phi - \theta) & mr_c^2 \end{bmatrix} \quad (3)$$

Equation of motion in flight phase

$$\ddot{x}_c = -g \quad (4)$$

$$\ddot{\phi} = 0 \quad (5)$$

$$\text{TD: } y_c + \frac{m}{m + m_f} r_c \sin(\phi) = l_0 \sin(\beta) \quad (6)$$

where  $z_c$  is the center of mass vertical position. With the initial positions and velocities of the point mass  $m$  and  $m_f$ , the initial condition  $[z_c, \dot{z}_c, \phi, \dot{\phi}]^T$  of the flight phase can be determined via linear and angular momentum conservation.

Dimension analysis:

- Mass is scaled by  $m$ :  $\tilde{m} = 1$ ,  $\tilde{m}_f = m_f/m$
- Length is scaled by  $l_0$ :  $\tilde{l} = l/l_0$ ,  $\tilde{r}_c = r_c/l_0$
- Time is scaled by  $l_0/v_0 \rightarrow \tilde{g} = gl_0/v_0$ ,  $\tilde{k} = kl_0^2/mv_0^2$

## 4 Simulations

### 4.1 1 DOF Vertical Hopper with Open-loop Control[11]

#### System Setup

- Body mass  $m = 1$  kg with massless leg,  $l = 1$  m.
- Spring parameters:  $\omega_n = 30$  rad/s,  $\xi = 0.15$  (or equivalently,  $kp = 900, kd = 9$ )
- Static initial condition, COM height = 1.3 m (foot to ground = 0.3 m)
- Open-loop external force:

$$f_n(t) = \begin{cases} f_n \in \mathbb{C}, & \text{if } t \in t_{on}. \\ 0, & \text{otherwise.} \end{cases}$$

- $t_{on}$ : The duration of actuator activation, starts when the spring reaches the maximum compression, ends when the contact point leave the ground.

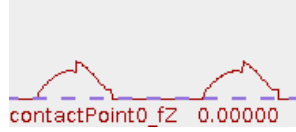


Figure 4: Ground reaction force when  $f_n = 10$  N

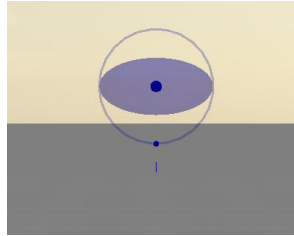


Figure 5: The vertical hopper, the blue dot at the bottom is the contact point of the massless leg.

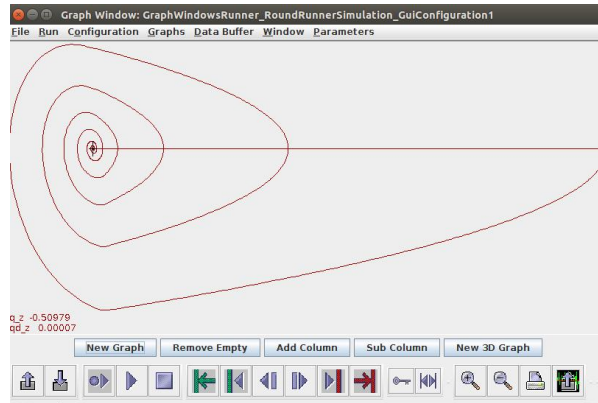


Figure 6: Phase portrait (stable spiral) of  $f = 1$  N, period 0 sec



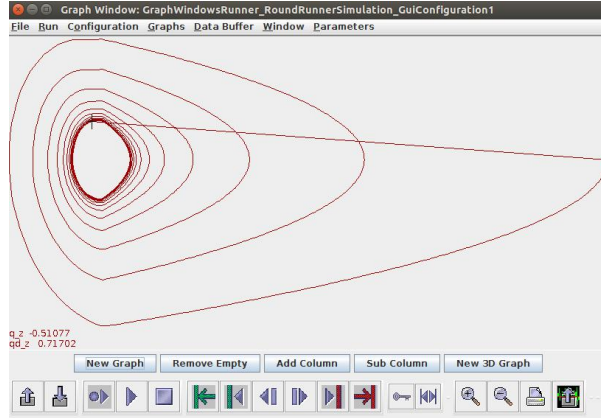


Figure 7: Phase portrait (stable limit cycle) of  $f = 10$  N, period 0.27sec, (closer to the damped natural period  $\cong 0.3295$  sec)

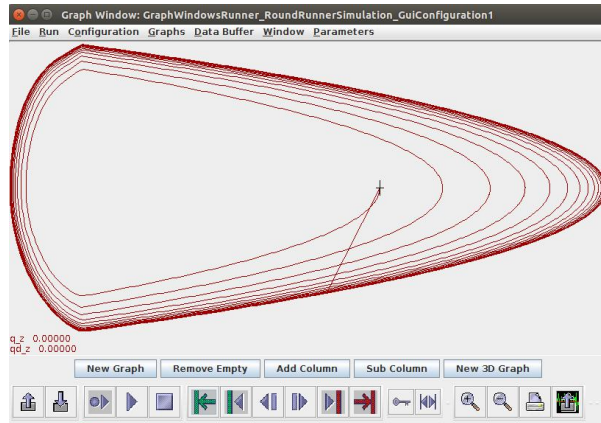


Figure 8: Phase portrait (stable limit cycle) of  $f = 50$  N, period 0.859 sec

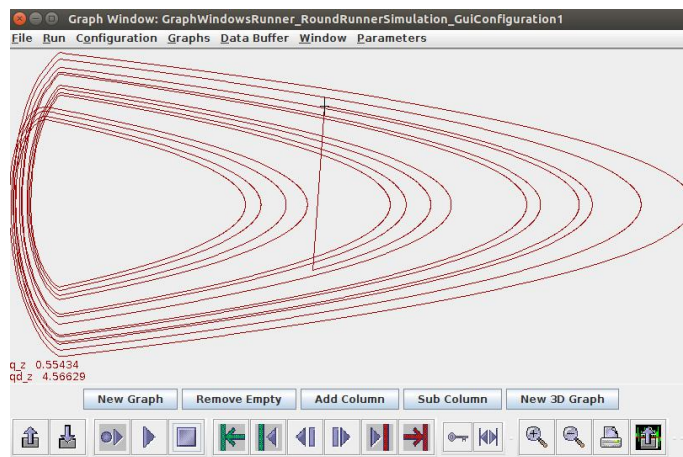


Figure 9: Phase portrait of  $f = 100$  N, no stable limit cycle evolved (might be bifurcation).

## Plan

- Go through and reuse the Poincare analysis in spokedReader package.

- Could be a good case for me to learn how to use parameterOptimizer (or other constrained nonlinear program solver) to get IC/parameters for a stable/optimal gait.

## 4.2 Abstract Runner with Open-loop Normal Force and Closed-loop Pitch Angle Control

### System Setup

- Body mass  $m = 10$ ,  $I_{yy} = 10$  with massless leg,  $l = 1$ .
- Reuse the vertical hopper above, change the initial condition to  $\theta = 0.2$
- No force applied in the x direction,  $\dot{x}_0$  can be 0 (hopper) or a constant (runner).
- Similar to the abstract runner (Fig. 10), enforces the on/off timing of ground reaction force  $f_n(t)$ :

$$f_n(t) = \begin{cases} (f_n + u)|f_n \in \mathbb{C}, & \text{if } t \in t_{on}. \\ 0, & \text{otherwise.} \end{cases}$$

where  $f_n = \alpha * mg$ ,  $\alpha \in \mathbb{C}$ ,  $u$  is the force from PD control,  $kp_z = 80, kd_z = 6$ .  $kp_{pitch} = 80, kd_{pitch} = 6$

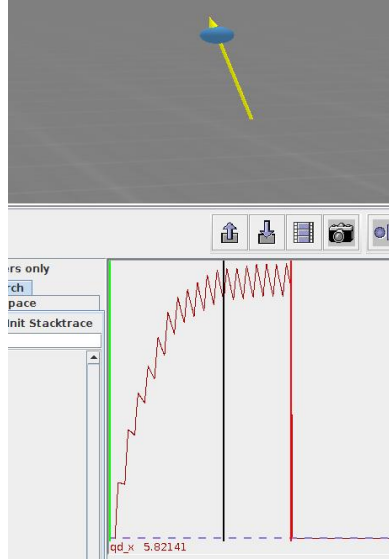


Figure 10: The Abstract Runner

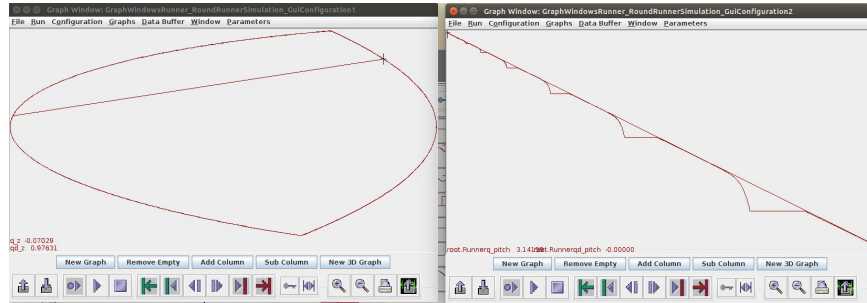


Figure 11: The phase portrait of the abstract runner: phase portrait (left) of body  $z$  movement  $[q_z, qd_z]^T$  and the pitch motion (right, the movement is converging to the origin in the upper-left corner) .

## Plan

- Link it to the Math from Jerry's note (analysis of a linear Poincare map) to get the boundaries of stable parameters.

## 4.3 Spoked Runner with Massless Legs

### System Setup

- $m = 15$ ,  $I_{yy} = 10$ ,  $l = 4$ ,  $r_{penetration} = 0.3$  (the distance the virtual wheel penetrate into the ground)
- Adjustable spoke leg number
- Fixed rotation rate w.r.t inertial frame
- Setup of contact force: PD control
  - w.r.t to world frame
  - w.r.t to inertial frame (virtual pivot point)
- Assuming no friction (Could be an bad idea?)

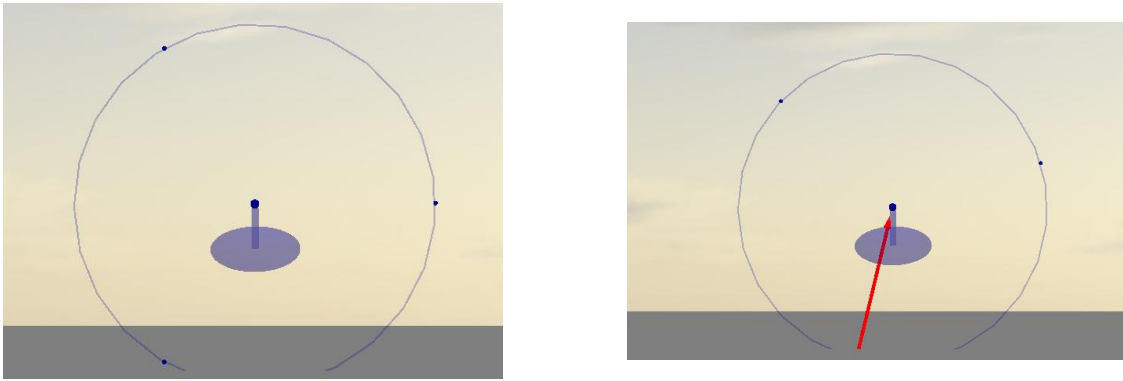


Figure 12: The Spoked Runner with three legs

## Plan

- Smoothly change the leg length, or the rotational speed of the virtual wheel, and observe the system response.
- Learn how to use GUI for parameter adjustment with SCS.

## 5 Code implementation

### 5.1 Modeling and Parameters

Main idea: a virtual wheel (as the massless leg) with radius  $r_{wheel}$  penetrate the ground for a distance  $r_{pen}$  where a external force point  $pe$  is attached on it. A body (with mass  $m$  and inertia  $I_{yy}$ ) is attached to the center of wheel. Using PD control to interpret contact force when  $p_e$  is under the ground.

#### 06/07 First prototype (Not used now)

- Joint numbers: 2
- Joint types: Floating planer joint for virtual wheel and pin joint for the body link.
- Contact point type: External force point
- Virtual wheel rotation: set proper initial condition for virtual wheel (also need a large inertia to make it nearly constant).

Contact force: Assuming the ground height is 0,

$$F_z = kp(0 - pe_z) + kd(0 - ve_z) \quad (1)$$

$$\phi = atan2(pe_x, r_{wheel} - pe_z) \quad (2)$$

$$F_x = F_z tan(\phi) \quad (3)$$

where  $ve$  is the velocity vector of the contact point  $pe$ ,  $kp$  and  $kd$  are the PD control parameters.  $F_x$  is calculated so that the vector of ground reaction force  $[F_x, F_y, F_z]^T$  will point towards the virtual pivot (the center of the virtual wheel).

Assessments:

- Need to set a non-zero inertia of massless virtual wheel (for numerical stability), otherwise the simulation will diverge.
- The inertia of virtual wheel need to be a large one for constant rotational speed.
- Suggestions: remove the massless link, attach the external force point to the body and change its position in the controller every time step.

#### 06/08 Round Runner

- Joint numbers: 1
- Joint types: Floating planer joint for the body link.
- Contact point type: External force point
- Virtual wheel rotation: Assigning the external force point location with respect to the joint in an open loop manner.
- Contact force: Assuming the ground height is 0,

$$F_z = kp(0 - pe_z) + kd(0 - ve_z) \quad (4)$$

$$\phi = atan2(pe_x, r_{wheel} - pe_z) \quad (5)$$

$$F_x = F_z tan(\phi) \quad (6)$$

where  $ve$  is the velocity vector of the contact point  $pe$ ,  $kp$  and  $kd$  are the PD control parameters.  $F_x$  is calculated so that the vector of ground reaction force  $[F_x, F_y, F_z]^T$  will point towards the virtual pivot (the center of the virtual wheel).

Assessments:

- The ground reaction force looks better, while the energy is not balanced (after a while it will move towards the negative  $x$  direction)
- The inertia of virtual wheel need to be a large one for constant rotational speed.
- Suggestions: Use the ground contact point (instead of external force point) to see how it goes.

#### 06/11 Round Runner(with Ground Contact Point)

- Joint numbers: 1
- Joint types: Floating planer joint for the body link.
- Contact point type: Ground contact point, linear contact model<sup>1</sup>
- Virtual wheel rotation: Assigning the external force point location with respect to the joint in an open loop manner.
- **Contact point number** Parameterized, currently set to 3-6 points.
- Contact force: using built-in functionalities, only assigning the  $kp$ ,  $kd$  (PD parameters in the  $z$  direction),  $kp_x$ , and  $kd_x$  (PD parameters in the  $x/y$  directions).

Assessments:

- Was able to generate a stable walking. Contact point has sliding.
- Due to setting up stiffness and damping for  $x$  and  $z$  separately, the force is not always point towards the virtual pivot.

#### 06/12 Round Runner(with External Contact Point Point)

- Implement the same one as 06/11, but replace the ground contact point to the external one (because it is more complex for ground contact point to adjust stiffness/damping as parameters.)
- implement the linear ground contact model basically.

#### 06/13 Round Runner

- Parameterize contact point numbers
- Adding enum for switching between different setup: contact point type and the corresponding ground reaction force calculation: (w.r.t to the world frame or inertia frame.)

#### 06/16 Round Runner (vertical hopper)

- Adding vertical hopper with open-loop force control
- Playing with open-loop force magnitudes for different stability conditions

---

<sup>1</sup>Disable the hardening stiffness in  $z$  direction by setting `groundStiffeningLength` to `Double.NEGATIVE_INFINITY`

## 6 Info might be useful

### 6.1 Finding a fixed-point solution from numerical Poincare map

If the analytical solution of Poincare map can be derived, then one can obtain the fixed-point easily. The followings are related methods (best to my knowledge) to get fixed-points of Poincare map through simulations:

#### Finding stable fixed-points

Take a collection of state at Poincare section defined (e.g. at touch down, or the end of the support phase, etc.) as  $[x_1, x_2, \dots, x_n]'$ . Take the first  $n - 1$  states as  $X_n = [x_1, x_2, \dots, x_{n-1}]'$  and the last  $n - 1$  states as  $X_{n+1} = [x_2, x_3, \dots, x_n]'$ , the map  $A$  can be approximated as:

$$\begin{aligned} X_{n+1} &= A(X_n) \\ \rightarrow A &= X_{n+1}/(X_n) \end{aligned}$$

If the system has a stable fixed point  $x^*$ , then the following should be satisfied:

$$\lim_{n \rightarrow \infty} x^* = x_n = Ax_{n-1} = A^n x_1 = x_{n-1}$$

Note:

- If  $A$  is invertible, the unstable fixed point might be derived by calculating the Poincare section in the backward manner.
- Whether the fixed-point is accurate enough is also depending on the quality of data (whether the data is sufficiently rich).
- Unlike the method like PCA, the data can only be subtracted by the fixed-point, otherwise the dynamics will be changed (scaling like dimensionless analysis is okay).

#### Finding fixed-points

The more general way to find fixed-point is to simulate the system, and evaluate the difference of the periodic condition at the Poincare section as the cost/constraint. Trajectory Optimization

- Single Shooting
- Multiple Shooting
- Direct Collocation

### 6.2 Going through references

1. Compare different terrestrial locomotions: Some parameters of the walk are not speed- dependent. The swing duration is a constant time parameter [1].
2. Trunk plays an important role during walking (birds) [2].
3. The use of these drives (Resonance drives, with adaptive control) allows increasing machine's quickness several times and decreasing energy expenses simultaneously 10-50 times [3].
4. Light weight leg (ostrich vs. moa) can run faster[5]. Also a famous allometric equation:

$$Y = M^{3/4} \tag{1}$$

where  $M$  is the body mass,  $Y$  is the metabolic rate.

5. Human's walking may not be really self-optimized: the preferred speed maybe different from the energetically optimal speed[8].

6. It is concluded that the most important adjustment to the bodys spring system to accommodate higher stride frequencies is that leg spring becomes stiffer [19].
7. magic equations for imd force (ostrich) [26]
8. gait frequency was reported to be highly correlated with the resonant frequency of the mass-spring model [30]
9. WABIAN, why you are here? [31]

### 6.3 Categories

1. Nonlinear oscillators/components [3, 6, 9, 10, 12, 28, 39];
2. zoology, biomechanics of animals: [1, 2, 4, 5, 16]
3. Bio-inspired robots: [7, 32]
4. Reference I should read: [11, 15, 27, 28]
5. Article not found (or not free)[4].
6. Robots in 3D: [13]
7. Stability analysis (Monocycle, linearized system) [14] (Limit cycle) [11, 27] dimensionless [41]
8. Biology/Anatomical structure [17, 20]
9. Light weight fast robot [18, 25]
10. take a look again [21]
11. mechanism design of robot [22]
12. quadruped reference [23] MIT Cheetah[37]
13. human energy cost, resonance usage [24, 8, 38, 40]
14. walking parameterization [29, 21, 42]
15. human-animal differences [15]
16. open-loop robot [33], passive robot [35, 34, 36]

## References

- [1] Anick Abourachid. Kinematic parameters of terrestrial locomotion in cursorial (ratites), swimming (ducks), and striding birds (quail and guinea fowl). *Comparative Biochemistry and Physiology Part A: Molecular and Integrative Physiology*, 131(1):113–119, dec 2001.
- [2] Anick Abourachid, Remi Hackert, Marc Herbin, Paul A. Libourel, François Lambert, Henri Gioanni, Pauline Provini, Pierre Blazevic, and Vincent Hugel. Bird terrestrial locomotion as revealed by 3D kinematics. *Zoology*, 114(6):360–368, dec 2011.
- [3] T. Akinfiyev and M. Armada. Elements of built-in diagnostics for resonance drive with adaptive control system. In *International Symposium on Automation and Robotics in Construction*, pages 617–621, Madrid, Spain, 1999.
- [4] R. Mc N Alexander, G. M O Maloiy, R. Njau, and A. S. Jayes. Mechanics of running of the ostrich (*Struthio camelus*). *Journal of Zoology*, 187(2):169–178, 1979.

- [5] R. McNeill Alexander. The legs of ostriches (Struthio) and moas (Pachyornis). *Acta Biotheoretica*, 34(2-4):165–174, 1985.
- [6] G. V. Anand. Nonlinear Resonance in Stretched Strings with Viscous Damping. *The Journal of the Acoustical Society of America*, 40(6):1517–1528, 1966.
- [7] Arvind Ananthanarayanan, Mojtaba Azadi, and Sangbae Kim. Towards a bio-inspired leg design for high-speed running. *Bioinspiration and Biomimetics*, 7(4):046005, dec 2012.
- [8] Elizabeth Arnall, Jessica Pyatt, Chelsie Rice, Katie L Anderson, and Duncan Mitchell. Resonance in Human Walking Economy: How Natural Is It? *International Journal of Undergraduate Research and Creative Activities*, 4(1), 2012.
- [9] V. I. Babitsky and M. Y. Chitayev. Adaptive high-speed resonant robot. *Mechatronics*, 6(8):897–913, dec 1996.
- [10] Jonas Buchli, Fumiya Iida, and Auke Jan Ijspeert. Finding resonance: Adaptive frequency oscillators for dynamic legged locomotion. In *IEEE International Conference on Intelligent Robots and Systems*, pages 3903–3909, Beijing, China, 2006.
- [11] J. G. Cham. *On Performance and Stability in Open-Loop Running*. PhD thesis, Stanford University, 2002.
- [12] S. Chatterjee and Anindya Malas. On the stiffness-switching methods for generating self-excited oscillations in simple mechanical systems. *Journal of Sound and Vibration*, 331(8):1742–1748, apr 2012.
- [13] Michael J. Coleman, Anindya Chatterjee, and Andy Ruina. Motions of a rimless spoked wheel: a simple three-dimensional system with impacts. *Dynamics and Stability of Systems*, 12(3):139–159, 1997.
- [14] Michael J. Coleman and Jim M. Papadopoulos. Intrinsic stability of a classical monocycle and a generalized monocycle. In *Bicycle and Motorcycle Dynamics, Symposium on Dynamics and Control of Single Track Vehicles*, Delft, Netherlands, 2010.
- [15] M. A. Daley and A. A. Biewener. Running over rough terrain reveals limb control for intrinsic stability. *Proceedings of the National Academy of Sciences*, 103(42):15681–15686, oct 2006.
- [16] M. A. Daley, G. Felix, and A. A. Biewener. Running stability is enhanced by a proximo-distal gradient in joint neuromechanical control. *Journal of Experimental Biology*, 210(3):383–394, feb 2007.
- [17] T. El-Mahdy, S. M. El-Nahla, L. C. Abbott, and S. A.M. Hassan. Innervation of the pelvic limb of the adult ostrich (Struthio camelus). *Journal of Veterinary Medicine Series C: Anatomia Histologia Embryologia*, 39(5):411–425, 2010.
- [18] Darrell Ethington. Dash Robotics Reveals A DIY High-Speed Running Robot Kit, Which Hobbyists Can Own For Just \$65, 2013.
- [19] Claire T. Farley and Octavio González. Leg stiffness and stride frequency in human running. *Journal of Biomechanics*, 29(2):181–186, 1996.
- [20] D. Gangl, G. E. Weissengruber, M. Egerbacher, and G. Forstenpointner. Anatomical description of the muscles of the pelvic limb in the ostrich (Struthio camelus). *Journal of Veterinary Medicine Series C: Anatomia Histologia Embryologia*, 33(2):100–114, 2004.
- [21] S. M. Gatesy and A. A. Biewener. Bipedal locomotion: effects of speed, size and limb posture in birds and humans. *Journal of Zoology*, 224(1):127–147, 1991.
- [22] Martin Grimmer and André Seyfarth. Design of a Series Elastic Actuator driven ankle prosthesis : The trade-off between energy and peak power optimization. In *Dynamic Walking*, 2011.



- [23] R Hackert, H Witte, and M S Fischer. Interactions between motions of the trunk and the angle of attack of the forelimbs in synchronous gaits of the pika (*Ochotona rufescens*). In *Adaptive Motion of Animals and Machines*, pages 69–77. Springer, 2006.
- [24] Kenneth G. Holt, Joseph Hamill, and Robert O. Andres. Predicting the minimal energy costs of human walking. *Medicine & Science in Sports & Exercise*, 23(4):491–498, 1991.
- [25] Fumiya Iida, Murat Reis, Nandan Maheshwari, Xiaoxiang Yu, and Amir Jafari. Toward efficient, fast, and versatile running robots based on free vibration. In *Dynamic Walking*, Pensacola, FL, 2012.
- [26] D. L. Jindrich, N. C. Smith, K. Jespers, and A. M. Wilson. Mechanics of cutting maneuvers by ostriches (*Struthio camelus*). *Journal of Experimental Biology*, 210(8):1378–1390, 2007.
- [27] Takahiro Kagawa and Yoji Uno. Necessary condition for forward progression in ballistic walking. *Human Movement Science*, 29(6):964–976, dec 2010.
- [28] Jg Daniël Karssen and Martijn Wisse. Running with improved disturbance rejection by using non-linear leg springs. *International Journal of Robotics Research*, 30(13):1585–1595, sep 2011.
- [29] Leng Feng Lee and Venkat N. Krovi. Musculoskeletal simulation-based parametric study of optimal gait frequency in biped locomotion. In *International Conference on Biomedical Robotics and Biomechatronics*, pages 354–359, Scottsdale, AZ, 2008.
- [30] Myunghyun Lee, Seyoung Kim, and Sukyung Park. Leg stiffness increases with load to achieve resonance-based CoM oscillation. In *Dynamic Walking*, Pittsburgh, PA, 2013.
- [31] Hun-ok Lim, Y Ogura, Atsuo Takanishi, and Proc R Soc A. Locomotion pattern generation and mechanisms of a new biped walking machine. *Proceedings of the Royal Society of London A: Mathematical and Physical Sciences*, 464(2089):273–288, 2008.
- [32] R. J. Lock, S. C. Burgess, and R. Vaidyanathan. Multi-modal locomotion: From animal to application. *Bioinspiration and Biomimetics*, 9(1), dec 2014.
- [33] Katja Mombaur, H Georg Bock, Johannes Schlöder, and Richard Longman. Stable Walking and Running Robots Without Feedback. In *Climbing and Walking Robots*, pages 725–735. 2005.
- [34] Dai Owaki, Masatoshi Koyama, Shin’ichi Yamaguchi, Shota Kubo, and Akio Ishiguro. A two-dimensional passive dynamic running biped with knees. In *Proceedings - IEEE International Conference on Robotics and Automation*, pages 5237–5242, 2010.
- [35] Dai Owaki, Masatoshi Koyama, Shin’ichi Yamaguchi, Shota Kubo, and Akio Ishiguro. A 2-D passive-dynamic-running biped with elastic elements. *IEEE Transactions on Robotics*, 27(1):156–162, 2011.
- [36] Dai Owaki, Koichi Osuka, and Akio Ishiguro. Understanding the common principle underlying passive dynamic walking and running. *2009 IEEE/RSJ International Conference on Intelligent Robots and Systems, IROS 2009*, pages 3208–3213, 2009.
- [37] Hae-won Park, Sangbae Kim, and Our Approach. Variable Speed Galloping Control using Vertical Impulse Modulation for Quadruped Robots : Application to MIT Cheetah Robot Click for Video Overview, 2012.
- [38] Sukyung Park. Can human walking be mimicked by resonance-based oscillation? In *The 7th World Congress on Biomimetics, Artificial Muscles and Nano-Bio*, volume 44, page 2013, Jeju Island, South Korea, 2013.
- [39] M C Plooi and M Wisse. A spring mechanism for resonant robotic arms. In *Workshop on Human Friendly Robotics*, page 5, 2011.
- [40] V. Racic, A. Pavic, and J. M.W. Brownjohn. Experimental identification and analytical modelling of human walking forces: Literature review. *Journal of Sound and Vibration*, 326(1-2):1–49, sep 2009.

- [41] Sebastian Riese and Andre Seyfarth. Stance leg control: Variation of leg parameters supports stable hopping. *Bioinspiration and Biomimetics*, 7(1):016006, mar 2012.
- [42] Robert E Weems. Locomotor Speeds and Patterns of Running Behavior in Non-Maniraptoriform Theropod Dinosaurs. *New Mexico Museum of Natural History and Science Bulletin*, 37:379–389, 2006.